ditional observations on a new type of pancreatic neoplasm. *Am J Surg Pathol* 2004; **28**: 233-238
20 **Kato N**, Akiyama S, Motoyama T. Pyloric gland-type tubular adenoma superimposed on intraductal papillary mucinous tumor of the pancreas. Pyloric gland adenoma of the pancreas. *Virchows Arch* 2002; **440**: 205-208
21 **Bakotic BW**, Robinson MJ, Sturm PD, Hruban RH, Offerhaus GJ, Albores-Saavedra J. Pyloric gland adenoma of the main pancreatic duct. *Am J Surg Pathol* 1999; **23**: 227-231
22 **Oh DK**, Kim SH, Choi SH, Jang KT. Intraductal tubular carcinoma of the pancreas: a case report with the imaging findings. *Korean J Radiol* 2008; **9**: 473-476
23 **Itatsu K**, Sano T, Hiraoka N, Ojima H, Takahashi Y, Sakamoto Y, Shimada K, Kosuge T. Intraductal tubular carcinoma in an adenoma of the main pancreatic duct of the pancreas head. *J Gastroenterol* 2006; **41**: 702-705
24 **Shahinian HK**, Sciadini MF, Springer DJ, Reynolds VH, Lennington WJ. Tubular adenoma of the main pancreatic duct. *Arch Surg* 1992; **127**: 1254-1255
25 **Sato Y**, Osaka H, Harada K, Sasaki M, Nakanuma Y. Intraductal tubular neoplasm of the common bile duct. *Pathol Int* 2010; **60**: 516-519
26 **Nakanuma Y**, Sato Y, Harada K, Sasaki M, Xu J, Ikeda H. Pathological classification of intrahepatic cholangiocarcinoma based on a new concept. *World J Hepatol* 2010; **2**: 419-427
27 **Tsutsumida H**, Swanson BJ, Singh PK, Caffrey TC, Kitajima S, Goto M, Yonezawa S, Hollingsworth MA. RNA interference suppression of MUC1 reduces the growth rate and metastatic phenotype of human pancreatic cancer cells. *Clin Cancer Res* 2006; **12**: 2976-2987
28 **Park SY**, Roh SJ, Kim YN, Kim SZ, Park HS, Jang KY, Chung MJ, Kang MJ, Lee DG, Moon WS. Expression of MUC1, MUC2, MUC5AC and MUC6 in cholangiocarcinoma: prognostic impact. *Oncol Rep* 2009; **22**: 649-657
29 **Gumbiner BM**. Signal transduction of beta-catenin. *Curr Opin Cell Biol* 1995; **7**: 634-640
30 **Kiesslich T**, Alinger B, Wolkersdörfer GW, Ocker M, Neureiter D, Berr F. Active Wnt signalling is associated with low differentiation and high proliferation in human biliary tract cancer in vitro and in vivo and is sensitive to pharmacological inhibition. *Int J Oncol* 2010; **36**: 49-58
31 **Sugimachi K**, Taguchi K, Aishima S, Tanaka S, Shimada M, Kajiyama K, Sugimachi K, Tsuneyoshi M. Altered expression of beta-catenin without genetic mutation in intrahepatic cholangiocarcinoma. *Mod Pathol* 2001; **14**: 900-905
32 **Itatsu K**, Zen Y, Ohira S, Ishikawa A, Sato Y, Harada K, Ikeda H, Sasaki M, Nimura Y, Nakanuma Y. Immunohistochemical analysis of the progression of flat and papillary preneoplastic lesions in intrahepatic cholangiocarcinogenesis in hepatolithiasis. *Liver Int* 2007; **27**: 1174-1184
33 **Abraham SC**, Lee JH, Hruban RH, Argani P, Furth EE, Wu TT. Molecular and immunohistochemical analysis of intraductal papillary neoplasms of the biliary tract. *Hum Pathol* 2003; **34**: 902-910

S- Editor Gou SX **L- Editor** Kerr C **E- Editor** Zhang DN

HEPATOLOGY
Official Journal of the American Association for the Study of Liver Diseases

Histological Diversity in Cholangiocellular Carcinoma Reflects the Different Cholangiocyte Phenotypes

Mina Komuta,[1] Olivier Govaere,[1] Vincent Vandecaveye,[2] Jun Akiba,[3] Werner Van Steenbergen,[4] Chris Verslype,[4] Wim Laleman,[4] Jacques Pirenne,[5] Raymond Aerts,[6] Hirohisa Yano,[3] Frederik Nevens,[4] Baki Topal,[6] and Tania Roskams[1]

Cholangiocellular carcinoma (CC) originates from topographically heterogeneous cholangiocytes. The cylindrical mucin-producing cholangiocytes are located in large bile ducts and the cuboidal non–mucin-producing cholangiocytes are located in ductules containing bipotential hepatic progenitor cells (HPCs). We investigated the clinicopathological and molecular features of 85 resected CCs (14 hilar CCs [so-called Klatskin tumor], 71 intrahepatic CCs [ICCs] including 20 cholangiolocellular carcinomas [CLCs], which are thought to originate from HPCs]) and compared these with the different cholangiocyte phenotypes, including HPCs. Immunohistochemistry was performed with biliary/HPC and hepatocytic markers. Gene expression profiling was performed in different tumors and compared with nonneoplastic different cholangiocyte phenotypes obtained by laser microdissection. Invasion and cell proliferation assay were assessed using different types of CC cell lines: KMC-1, KMCH-1, and KMCH-2. Among 51 ICCs, 31 (60.8%) contained only mucin-producing CC features (muc-ICCs), whereas 39.2% displayed histological diversity: focal hepatocytic differentiation and ductular areas (mixed-ICCs). Clinicopathologically, muc-ICCs and hilar CCs showed a predominantly (peri-)hilar location, smaller tumor size, and more lymphatic and perineural invasion compared with mixed-ICCs and CLCs (predominantly peripheral location, larger tumor size, and less lymphatic and perineural invasion). Immunoreactivity was similar in muc-ICCs and hilar CCs and in mixed-ICCs and CLCs. *S100P* and *MUC1* were significantly up-regulated in hilar CCs and muc-ICCs compared with mixed-ICCs and CLCs, whereas *NCAM1* and *ALB* tended to be up-regulated in mixed-ICCs and CLCs compared with other tumors. KMC-1 showed significantly higher invasiveness than KMCH-1 and KMCH-2. *Conclusion*: Muc-ICCs had a clinicopathological, immunohistochemical, and molecular profile similar to that of hilar CCs (from mucin-producing cholangiocytes), whereas mixed-ICCs had a profile similar to that of CLCs (thought to be of HPC origin), possibly reflecting their respective cells of origin. (HEPATOLOGY 2012;55:1876-1888)

Cholangiocellular carcinoma (CC) is a primary liver tumor originating from cholangiocytes (epithelial cells that line the bile duct). Cholangiocytes are topographically heterogeneous within the different levels of the biliary tree.[1] The biliary tree is divided anatomically into extra- and intrahepatic bile duct (BD). Hilar BD and right and left hepatic BD are considered extrahepatic BD, and they are lined by cylindrical mucin-producing cholangiocytes. Inside the liver, a large intrahepatic BD (such as segmental, area, and septal BD) has a lining of similar mucin-producing cylindrical cells, whereas a small intrahepatic BD (such as interlobular BD and ductules) is lined with mucin-negative cuboidal cholangiocytes. In addition, ductules contain hepatic progenitor cells (HPCs),[2] which can differentiate into both hepatocytes

Abbreviations: ANXA3, annexin A3; BD, bile duct; CC, cholangiocellular carcinoma; CLC, cholangiolocellular carcinoma; DR, ductular reaction; EMA, epithelial membrane antigen; EpCAM, epithelial cell adhesion molecule; HCC, hepatocellular carcinoma; hep-dif, hepatocytic differentiation; HPC, hepatic progenitor cell; ICC, intrahepatic CC; mixed-ICC, ICC with mixed features; MRI, magnetic resonance imaging; muc-ICC, mucin-producing ICC; NCAM, neural cell adhesion molecule; pCEA, polyclonal carcinoembryonic antigen; PSC, primary sclerosing cholangitis; RT-PCR, reverse-transcription polymerase chain reaction; TACSTD2, tumor-associated calcium signal transducer 2; WHO, World Health Organization.

From the Departments of [1]Morphology and Molecular Pathology, [2]Radiology, [4]Hepatology, [5]Abdominal Transplant Surgery, and [6]Abdominal Surgery, University Hospitals Leuven, Leuven, Belgium; and the [3]Department of Pathology, Kurume University School of Medicine, Fukuoka, Japan

Received July 30, 2011; accepted December 23, 2011.

Supported by an Interuniversity Attraction Pole (IUAP) grant from Belspo Belgium.

and cholangiocytes and can give rise to tumors during the differentiation process.[3] HPC-derived tumors can display varying hepatocytic and/or cholangiocytic differentiation characteristics within the same tumor. For example, cholangiolocellular carcinoma (CLC), a subtype of intrahepatic CC (ICC), is reported as an HPC-derived tumor showing histological diversity with hepatocytic and/or cholangiocytic differentiation characteristics.[4] Therefore, we hypothesized that the different cholangiocyte phenotypes could lead to different clinicopathological phenotypes of CC. Mucin-producing cylindrical cholangiocytes could lead to mucin-producing CC such as hilar CC (Klatskin tumor), whereas mucin-negative cuboidal cholangiocytes, including HPCs, could give rise to tumors with histological variation, such as hepatocytic and cholangiocytic differentiation characteristics (as in CLC).

World Health Organization (WHO) classification is based on the original location (BD) of the tumor.[5] CC arising from the right and left hepatic ducts, at or near their junction, is called hilar CC (Klatskin tumor) and is considered an extrahepatic lesion. CC arising from the intrahepatic large BDs (intrahepatic second branches or segmental branches) is called peri-hilar ICC and is considered an intrahepatic lesion.[5] We anticipate that hilar CC and peri-hilar ICC could have a similar tumor profile, because they arise from similar mucin-producing cholangiocytes. In addition, liver hilum is a location of hilar CC and peri-hilar CC, because large BD locates mainly in the liver hilum. However, the biliary system inside the liver has a three-dimensional tree-like structure, harboring small ducts in the hilar as well as in the peripheral subcapsular regions. Therefore, liver hilum has the potential to contain an HPC-derived ICC that shows histological diversity, as well as peri-hilar CC. We hypothesize that different CC phenotypes may reflect the cholangiocyte phenotype and can thus resolve the issues of the current anatomical-based classification of CC.[5,6] As the recent incidence and associated mortality of CC has been increasing, the need for a review of the current anatomical-based classification has become evident. The current classification system does not allow accurate assessment of epidemiological background and patient outcome with CC.

We investigated 85 CCs, including 14 hilar CCs and 20 CLCs, and compared their clinicopathological features with the different nonneoplastic cholangiocytes. We correlated the immunohistochemistry and gene expression profiling of the nonneoplastic cholangiocytes with clinicopathological characteristics of the different CCs.

Patients and Methods

Patient Selection. We examined 85 consecutively resected CCs between 1991 and June 2011 (46 men, 39 women; mean age, 63.3 years) comprising 83 surgical resections and two explant livers. CCs were diagnosed by clinical and radiological data and confirmed with histological examination. The histological diagnosis was made according to WHO criteria.[5] The tumor staging was made according to 7th edition of the American Joint Committee on Cancer/Union for international Cancer Control TNM classification.[6] The specimens were treated and investigated as described.[4] Tumor location was classified based on surgical findings, macroscopic examination, and imaging studies, including computed tomography, magnetic resonance imaging (MRI), and endoscopic retrograde cholangiopancreaticography, when available.[5,7] Macroscopic type of ICCs was investigated according to the Liver Cancer Study Group of Japan.[8] This study was approved by the Local Commission for Medical Ethics.

Immunohistochemistry. Immunohistochemistry was performed on paraffin-embedded sections using a large BD marker (S100P)[9] epithelial membrane antigen (EMA, MUC1), HPC/biliary markers (K7, K19, neural cell adhesion molecule [NCAM],[10] tumor-associated calcium signal transducer 2 [TACSTD2, TROP2],[11] epithelial cell adhesion molecule [EpCAM, TACSTD1, TROP1],[12] and annexin A3 [ANXA3][13]), and hepatocytic markers (Hep Par 1, and canalicular polyclonal carcinoembryonic antigen [pCEA]) (Supporting File 1). The slides were reviewed by two independent pathologists (M. Komuta and T. Roskams). Immunoreactivity was considered positive if more than 1% of tumor cells were stained in the proper pattern. TACSTD2 overexpression was scored as described before.[14]

Address reprint requests to: Mina Komuta, M.D., Laboratory of Morphology and Molecular Pathology, Minderbroederstraat 12, 3000 Leuven, Belgium. E-mail: mina.komuta@gmail.com; fax: (32)-16-336548.

View this article online at wileyonlinelibrary.com.

DOI 10.1002/hep.25595

Potential conflict of interest: Nothing to report.

Additional Supporting Information may be found in the online version of this article.

Real-Time Quantitative Reverse-Transcription Polymerase Chain Reaction of Tumor Samples. Five hilar CCs, six mucin-producing ICCs (muc-ICCs), seven ICCs with mixed features (mixed-ICCs), and seven CLCs were included for reverse-transcription polymerase chain reaction (RT-PCR) analysis for the following genes: *KRT19/7*, *ANXA3*, *TACSTD2*, *EpCAM*, *NCAM1*, *ALB*, *S100P*, and *MUC1*. Sequences and a detailed protocol are listed in Supporting File 2.

Invasion Assay and Cell Proliferation Assay Using Cell Lines. Three different human CC cell lines, KMC-1, KMCH-1, and KMCH-2, which were originally established at the Department of Pathology, Kurume University School of Medicine, were used. KMC-1 was established from an intrahepatic-CC observed as a tubular adenocarcinoma with mucin production.[15] KMCH-1 was established from a combined hepatocellular-cholangiocarcinoma comprising both a hepatocellular carcinoma (HCC) area and a CC area.[16] KMCH-2 was established from a combined hepatocellular cholangiocarcinoma showing intermediate features between HCC and CC.[17] These cell lines were previously confirmed to retain the morphological and functional characteristics of the original tumor. The invasive ability *in vitro* was measured by using BD BioCoat Matrigel Invasion Chambers (BD Bioscience, Bedford, MA). The growth of cultured cells was examined with colorimetry using the MTT assay kit (Chemicon International Inc., Temecula, CA). Further information is provided in Supporting File 3.

Microdissection of Hilar BD, Segmental BD, and Ductular Reaction. Human liver specimens from liver explants and resections taken for diagnostic purposes were used in this study, including hilar BD lined with mucin-secreting cholangiocytes (n = 6) and segmental BD lined with mucin-secreting cholangiocytes (n = 4) which were obtained from normal looking hilar and segmental BDs at a distance of a benign tumor, and activated HPCs/ductular reaction (DR) (n = 8) obtained from HCV-related chronic hepatitis (n = 4) and primary sclerosing cholangitis (PSC)-related chronic biliary disease (n = 4). Tissue samples were obtained using the laser capture microdissection LMD6500 system (Leica Microsystems, Wetzlar, Germany). Further information is provided in Supporting File 4.

Preoperative MRI. Forty-six MRI studies were available for evaluation and reviewed by an expert abdominal radiologist in a blinded manner. Further information is provided in Supporting File 5.

Clinical Outcome. Nine of the 85 patients were excluded from survival analysis for the following reasons: two patients were lost to follow-up, and seven patients died in hospital from liver failure, multiple organ failure, or bleeding. Thus, 76 patients were ultimately analyzed for survival and outcome. Overall survival was defined as the interval between treatment and death, or the date of the last or most recent follow-up. Recurrence-free survival was defined as the interval between treatment and the date of recurrence, which was monitored by clinical and imaging assessment, until the patient's death, or the end of the study. Survival curves were computed according to the Kaplan-Meier method and compared using the log-rank test.

Statistical Analysis. Continuous data are expressed as the mean ± SD. Detection of significances between the four groups was done using chi-square and Kruskal-Wallis analysis of variance for categorical and continuous data, respectively. Post hoc comparisons between groups were performed using chi-square and Mann-Whitney U tests, with Bonferroni correction for multiple testing. Analysis was performed using GraphPad Prism software (GraphPad Software, Inc., CA). $P < 0.05$ was considered statistically significant.

Results

Histopathological Variation in Hilar CCs, Intrahepatic CCs, and CLCs. Using the WHO classification, 85 CCs were classified into 14 (16.5%) hilar CCs and 71 (83.5%) intrahepatic CCs (ICCs) (Fig. 1). Among the 71 intrahepatic ICCs, 20 (28.2%) were diagnosed as CLCs.[4] Of the remaining 51 ICCs, 31 (60.8%) comprised pure mucin-producing adenocarcinomas (muc-ICCs), and the other 20 (39.2%) exhibited features of predominant mucin-producing adenocarcinoma with histological diversity (hepatocytic differentiation areas [hep-dif] and/or ductular areas in the tumor [mixed-ICC]). A hep-dif area was defined as a thick trabecular and/or solid growth pattern with little stroma, and tumor cells with abundant eosinophilic cytoplasm, mild atypia, and no mucin production. Hepatocytic differentiation (hep-dif) areas were always located at the tumor boundary, proliferating as if it was replacing the surrounding liver cell cords, and associated with lymphoid infiltration. A ductular area was characterized by ductular reaction-like anastomosing glands in edematous fine fibrous stroma with mild atypia, no mucin production, and cuboidal tumor cells. In contrast with hep-dif areas, ductular areas and mucin-producing adenocarcinoma were mainly seen in the center of the tumor with abundant fibrous stroma. This histological diversity, which was seen in mixed-

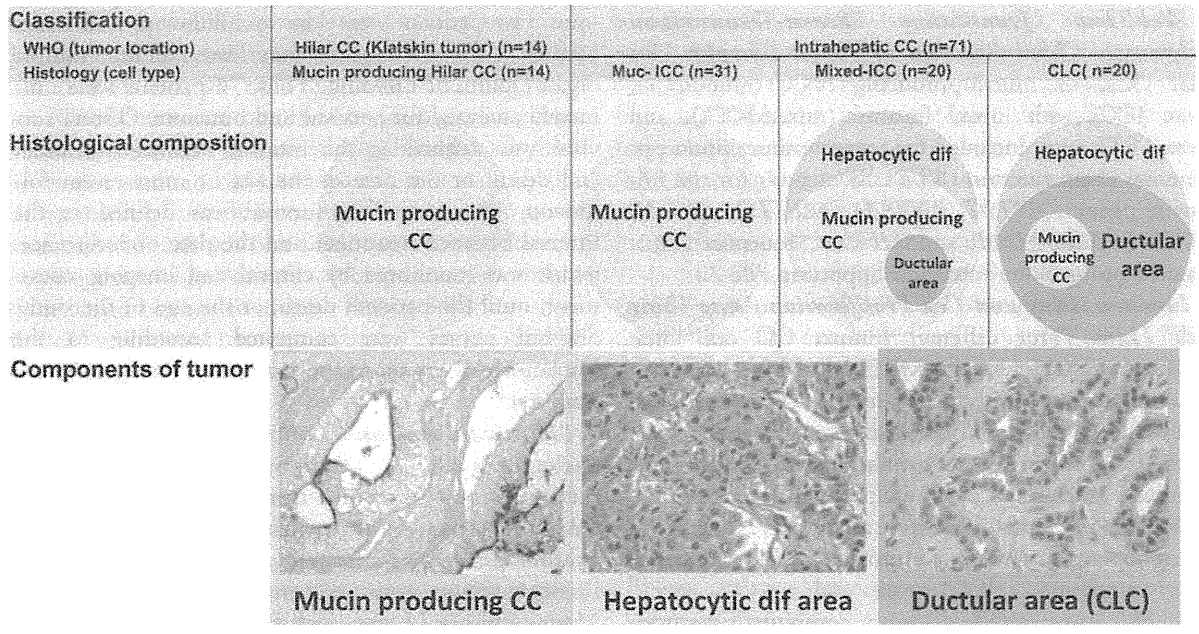

Fig. 1. Histological variation of 14 hilar CCs and 71 ICCs, including 20 CLCs. All hilar CCs and 31 ICCs (muc-ICCs) showed only mucin-positive CCs, whereas 20 mixed-ICCs and 20 CLCs contained mixed histological features (hepatocytic differentiated areas and/or ductular areas).

ICCs, has been already described in CLCs.[4] Thus, mixed-ICC and CLC have overlapping histopathological aspects. Ductular areas have been described as a typical feature of CLC.[4] The only difference between mixed-ICC and CLC was the predominant feature: where CLC showed ductular areas in more than 90% of the tumor, mixed-ICCs showed predominant mucin producing CC with focal hep-dif and/or ductular areas.

We further investigated the clinicopathological features and gene expression profiling of 14 hilar CCs, 31 muc-ICCs, 20 mixed-ICCs and 20 CLCs (based on histological classification).

Clinicopathomorphological Findings in Hilar CCs, Muc-ICCs, Mixed-ICCs, and CLCs Etiology. The etiology of underlying liver disease is listed in Table 1. Although there were no significant differences, hepatitis B or C infection was seen mainly in mixed-ICCs and CLCs compared with hilar CCs and muc-ICCs, while PSC was seen primarily in muc-ICCs/hilar CCs.

Gross Findings. All hilar CCs were located in the liver hilum. About 77% of the muc-ICCs were located in the perihilar area, while 80% of the mixed-ICCs and 75% CLCs were located in the peripheral area ($P < 0.05$). All mixed-ICCs and CLCs showed a mass forming growth pattern, while muc-ICCs showed both a mass-forming growth pattern and a combination of a mass-forming growth pattern with a periductal infiltrative growth pattern. All hilar CCs and more than 90% of muc-ICCs were a single tumor, whereas around 20% of mixed-ICCs and CLCs were multiple tumors. Tumor size was significantly smaller in hilar CCs and muc-ICCs compared with mixed-ICCs and CLCs. All 85 CCs underwent surgery with curative intent. Positive microscopic resection margin was seen in two (14.3%) hilar CCs, six (19.4%) muc-ICCs, one (5%) mixed-ICC, and two (10%) CLCs.

Histological Findings. All hilar CCs and 27 (87.1%) muc-ICCs showed secondary cholangitis associated with parenchymal necrosis/inflammation. Bile duct dysplasia in surrounding nontumoral liver tissue was significantly seen in hilar CCs compared with mixed-ICCs and CLCs. Hilar CCs and muc-ICCs showed mucin-producing adenocarcinoma of predominantly well to moderate differentiation. On the other hand, mixed-ICCs and CLCs could not be categorized based on tumor differentiation because of their histological diversity. Lymphatic and perineural invasion were significantly higher in hilar CCs and muc-ICCs compared with mixed-ICCs and CLCs. Hilar CCs and muc-ICCs showed similar histopathological aspects, whereas CLCs and mixed-ICCs were histologically overlapping.

These different cancer areas correlated with the different types and amount of stroma (Supporting Fig.1).

Table 1. Clinicopathological Features of Hilar CC and ICC

WHO Classification	Hilar CC (Klatskin Tumor; n = 14)	ICC (n = 71)			
Histological Classification	Hilar CC (n = 14)	Muc-ICC (n = 31)	Mixed-ICC (n = 20)	CLC (n = 20)	*P* Value
Age, years, range (mean ± SD)	40-77 (59.1 ± 10.6)	26-85 (62.9 ± 14.4)	50-84 (64.1 ± 9.9)	48-79 (64.2 ± 8.8)	0.9831
Sex, male/female	9/5	17/14	12/8	8/12	0.4801
Etiology					
HBsAg- or HCVAB-positive	1 (7.1)	1 (3.2)	3 (15.0)	2 (10.0)	
PSC	1 (7.1)	4 (13.0)	1 (5.0)	0 (0)	
(Non-)alcoholic steatohepatitis	0 (0)	1 (3.2)	2 (10.0)	3 (15.0)	
Other	0 (0)	0 (0)	1[*] (5.0)	2[‖] (10.0)	
No underlying liver disease	12 (85.8)	25 (80.6)	13 (65.0)	13 (65.0)	
Tumor location (WHO)*					<0.0001
Hilar (extrahepatic)	14 (100)	0 (0)	0 (0)	0 (0)	
Perihilar (intrahepatic)	0 (0)	24 (77.4)	4 (20.0)	5 (25.0)	
Periphery (intrahepatic)	0 (0)	7 (22.6)	16 (80.0)	15 (75.0)	
Stage (AJCC/UICC)[†]					
I	0	3 (9.7)	6 (30.0)	3 (15.0)	
II	11[†]	14 (45.2)	11 (55.0)	11 (55.0)	
III	3 (IIIB)[†]	2 (6.4)	0	3 (15.0)	
IVa	0	12 (38.7)	3 (15.0)	3 (15.0)	
Macroscopic finding					
MF		14	20	20	
PI		0	0	0	
IG		2	0	0	
MF+PI		13	0	0	
MF+IG		2	0	0	
Number of nodules					0.0819
1	14 (100)	29 (93.5)	15 (75.0)	16 (80.0)	
≥2	0 (0)	2 (6.5)	5 (25.0)	4 (20.0)	
Tumor size (mm)					<0.0001
Range (mean ± SD)	10-40 (23.1 ± 9.2)	8-120 (41.2 ± 26.2)	20-125 (67.3 ± 28.6)	20-170 (64.6 ± 35.2)	
<20	7	5	1	1	
21-30	5	11	2	1	
31-40	2	5	1	2	
41-50	0	3	3	7	
≥50	0	7	13	9	
Histological findings					
BD dysplasia[‡]	8 (57.1)	10 (32.3)	3 (15)	2 (10.0)	0.0104
Vascular invasion	10 (71.4)	26 (83.9)	12 (60.0)	15 (75.0)	0.2986
Lymphatic invasion	13 (92.9)	27 (87.1)	12 (60.0)	9 (45.0)	0.0017
Perineural invasion	13 (92.9)	25 (80.7)	9 (45.0)	10 (50.0)	0.0031
Lymph node involvement	3/13 (23.1)	12/22 (54.5)	3/12 (25.0)	3/14 (21.4)	0.1020
Immunohistochemistry					
S100P-positive	14 (100)	30 (96.8)	0 (0)	0 (0)	<0.0001
TACSTD2 overexpression	11 (78.6)	30 (96.8)	10 (50.0)	8 (40.0)	<0.0001

Abbreviations: AJCC/UICC, American Joint Cancer Committee/Union Internationale Contrele-Cancer; HBsAg, hepatitis B surface antigen; HCVAB, hepatitis C virus IG, intraductal growth; MF, mass-forming; PI, periductal infiltrative.

Data are presented as no. (%) unless indicated otherwise.

*Tumor location was defined by WHO classification.

[†]Hilar CC was staged according to extrahepatic BD cancer classification; the others were staged according to intrahepatic BD cancer classification.

‡BD dysplasia in the surrounding nontumoral liver tissue.

[§]Hemochromatose (n = 1).

[‖]Hemochromatose (n = 1), α1-antitrypsin-deficient (n = 1).

Hep-dif areas contained a small amount of fine fibrosis located around the tumor nests and were associated with lymphocytic inflammation and narrow blood spaces. In contrast, mucin-producing CC areas showed hyalinizing, abundant, dense fibrous stroma occupying around 40%-50% of the area. Lymphocytic infiltration in the stroma became more prominent in cases of BD obstruction, which gave rise to abscess formation and lymphocyte infiltration associated with lymphoid follicles. Ductular areas showed mainly edematous fibrous stroma accompanied by lymphocytic infiltration that occupied approximately 30%-50% of the area. Hep-dif areas and ductular areas were seen in varying degree in the tumor, and they showed transitional zones between each other and with the mucin-producing adenocarcinoma area.

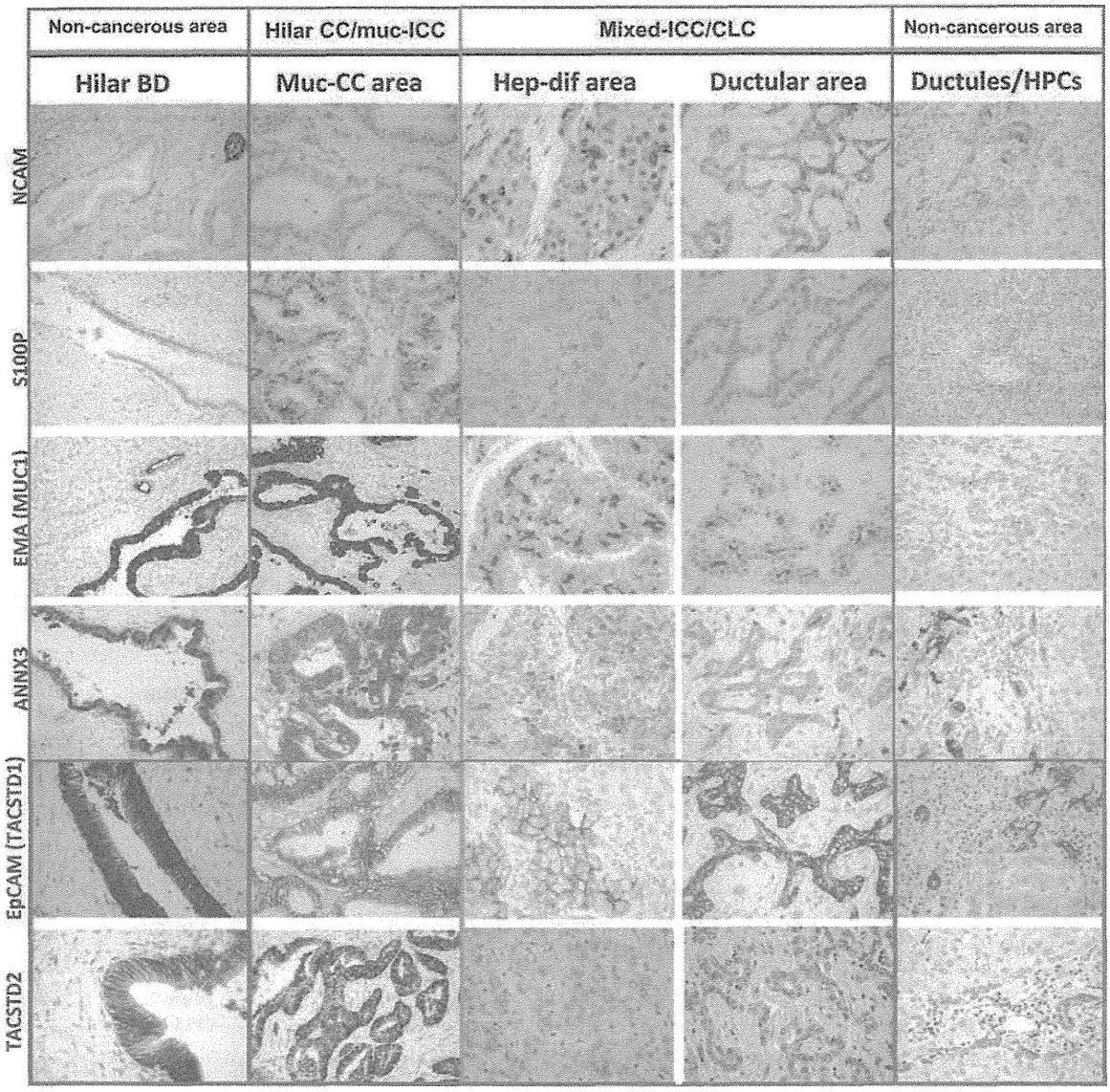

Fig. 2. Immunohistochemical profiles in different tumor types compared with different levels of the BD. Mucin-producing CC area in hilar CCs and muc-ICCs showed similar immunohistochemical profiles to hilar BD, which showed cytoplasmic/nuclear positivity for S100P and intense cytoplasmic positivity for EMA, ANNX3, EpCAM, and TACSTD2, and no positivity for NCAM. Ductular areas in mixed-ICCs and CLCs showed a similar immunohistochemical profile to ductules/HPCs with membranous positivity for NCAM, cytoplasmic positivity for ANNX3, EpCAM, and TACSTD2, and apical positivity for EMA. Hep-dif showed focal positivity for NCAM, ANNX3, and TACSTD2, membranous positivity for EpCAM, and canalicular-like/cytoplasmic positivity for EMA. S100P expression was negative in the hep-dif and ductular areas.

Immunohistochemical Profiles of Different Tumors (Hilar CCs, Muc-ICCs, Mixed-ICCs, and CLCs) Compared with Normal Counterparts (Hilar BD and Ductules/ HPCs). Mucin-positive CC areas in hilar CCs and muc-ICCs showed similar immunohistochemical staining patterns to hilar BD, with cytoplasmic/nuclear positivity for S100P, intense cytoplasmic positivity for EMA, ANNX3, EpCAM, and TACSTD2, and no positivity for NCAM (Fig. 2). Mucin-positive CC areas (n = 30) in mixed-ICCs and CLCs showed similar immunoprofiles to those areas from hilar CCs and muc-ICCs, apart from S100P immunoreactivity. S100P expression was seen only in mucin-positive CC areas in hilar CCs and muc-ICCs, but not in the mixed-ICCs and CLCs.

Ductular areas in mixed-ICCs and CLCs showed similar immunohistochemical profiles to ductules/HPCs; they demonstrated membranous positivity for

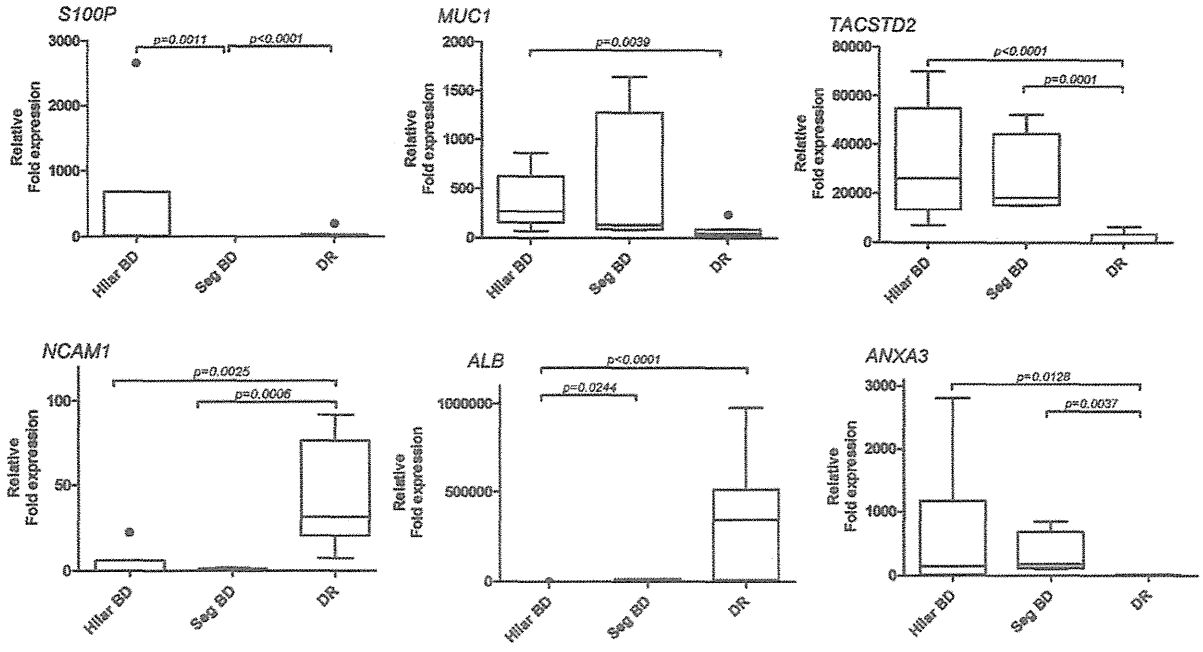

Fig. 3. Gene expression profiling. Box plots of RT-PCR results for biliary markers (*S100P* and *MUC1*), HPC/biliary markers (*NCAM1*, *ANXA3*, and *TACSTD2*), and hepatocytic marker *ALB* (hilar BD, n = 6; segmental BD, n = 4; DR, n = 8).

NCAM, cytoplasmic positivity for ANNX3, EpCAM, and TACSTD2, and apical positivity for EMA. S100P was negative in both the ductular areas of mixed-ICCs and CLCs and ductules/HPCs.

Hep-dif areas showed focal positivity for NCAM, ANNX3, and TACSTD2, membranous positivity for EpCAM, a canalicular/abberrant canalicular pattern for pCEA, and canalicular-like/cytoplasmic positivity for EMA in mixed-ICCs and CLCs. Focal Hep Par 1 expression was seen in 11 (55%) mixed-ICCs and 16 (80%) CLCs. S100P expression was negative in the hep-dif area.

Gene Expression Profiling of Hilar CCs, Muc-ICCs, Mixed-ICC, and CLCs Compared with Different Levels of BD. We investigated six hilar BDs, four segmental BDs, and eight DRs obtained using laser capture microdissection (Fig. 3, Supporting Fig.2). *TACSTD2* and *ANXA3* showed significantly higher expression in hilar and segmental BD compared with DR, whereas *NCAM1* was significantly higher in DR compared with hilar and segmental BD. *MUC1* was significantly stronger in hilar BD compared with DR, whereas *ALB* showed significantly higher expression in DR compared with hilar BD. Among different levels of BD, hilar BD has more similar profiles with segmental BD compared with DR. For a comparison of different tumors, we investigated five hilar CCs, six muc-ICCs, seven mixed-ICCs, and seven CLCs (Fig. 4, Supporting Fig. 3). *S100P* and *MUC1* were significantly up-regulated in hilar CCs and muc-ICCs compared with mixed-ICCs and CLCs, whereas *NCAM1* and *ALB* tended to be up-regulated in mixed-ICCs and CLCs compared with other tumors. *KRT19* and *EpCAM* were significantly up-regulated in mixed-ICCs compared with hilar CCs, but their immunohistochemical expression (on protein level) was similar.

Invasion Assay and MTT Assay Using Cell Lines. The morphological features of KMC-1, KMCH-1, and KMCH-2 were identical to those described.[15-17] Based on the pathology of their original tumors, and cellular features of the cell line, KMC-1 was thought to correspond to muc-ICCs, and KMCH-1 and KMCH-2 were thought to be representative for the mixed-ICCs. KMC-1, corresponding to muc-ICCs, showed significantly higher invasiveness compared with KMCH-1 and KMCH-2 (corresponding to the mixed-ICCs) ($P < 0.01$) (Fig. 5). In contrast, KMCH-1 and KMCH-2 showed a significantly higher proliferation rate at 72 hours and 96 hours compared with KMC-1 ($P < 0.001$).

Preoperative MRI: Lesion Characteristics. Forty-six MRI studies correlated histologically with 8 hilar CCs, 14 muc-ICCs, 10 mixed-ICCs, and 14 CLCs. Hilar CCs presented as a small mass or enhancing biliary wall at the extrahepatic hepatic ducts and/or their bifurcation with the main BD. Detailed results for the

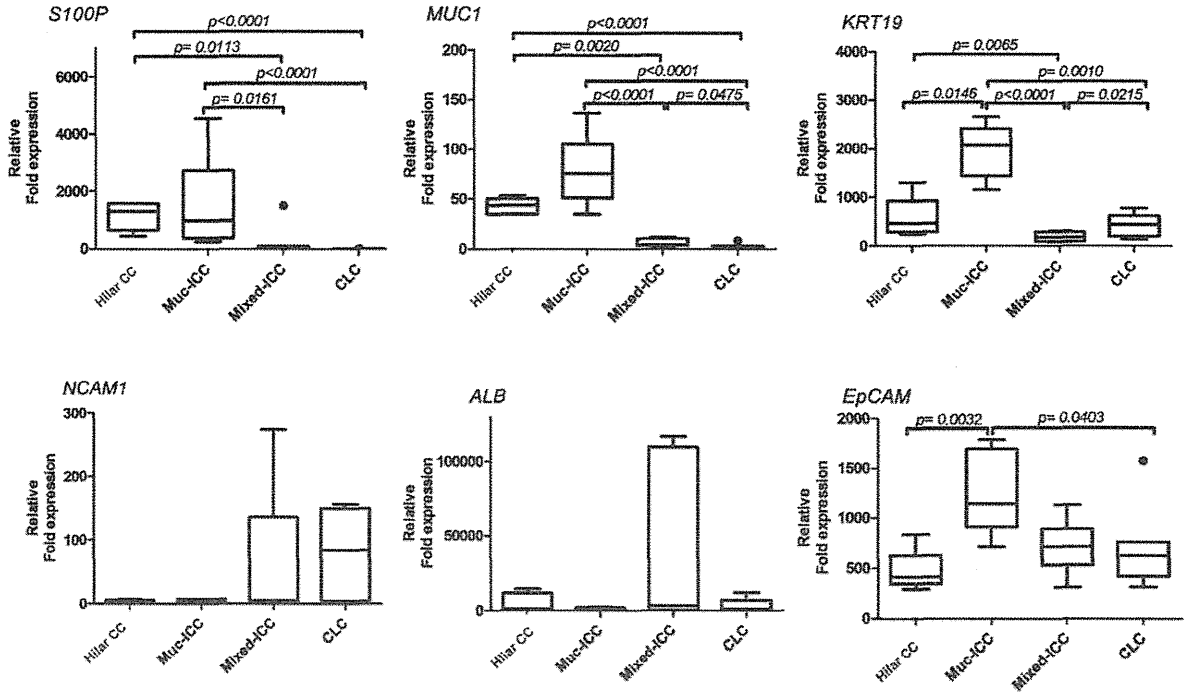

Fig. 4. Gene expression profiling. Box plots of RT-PCR results for HPC/biliary markers (*KRT19*, *NCAM1*, and *EpCAM*), biliary markers (*S100P* and *MUC1*), and hepatocytic marker *ALB* (hilar CCs, n = 5; muc-ICCs, n = 6; mixed-ICCs, n = 7; CLCs, n = 7).

intrahepatic tumors are summarized in Fig. 6. Briefly, all muc-ICCs showed homogeneous T2 intensity, whereas 70% of mixed-ICCs and 86% of CLCs showed mixed intensity, in concentric (peripheral hyperintense-central hypointense) or random nodular distribution. At dynamic contrast-enhanced imaging, all muc-ICCs showed concentric filling at venous phase, whereas mixed-ICCs/CLCs showed washout in various patterns. Historadiological comparison between muc-ICC and CLC is shown in Fig. 7.

Clinical and Follow-up Data. Seventy-six surgically treated patients (11 hilar CCs, 29 muc-ICCs, 18 mixed-ICCs, and 18 CLCs) were available for follow-up data (33-4,654 days, 833.3 ± 807.8). There was no statistically significant difference in recurrence-free survival days and overall survival days in these four groups. However, the hilar CC and muc-ICC groups tended to show worse prognosis compared with the mixed-ICC and CLC groups (Supporting Fig. 4).

Discussion

Cholangiocytes, which line the BDs, show topographic heterogeneity within the different levels of the biliary tree.[1] The heterogeneity of cholangiocytes is most distinct when comparing the smallest, mucin-negative cuboidal cholangiocytes located in the canal of Hering/ductules and the taller, cylindrical, mucin-producing cholangiocytes located in the larger BDs. The smallest cholangiocytes include hepatic progenitor cells (HPCs), which are able to differentiate into both hepatocytes and cholangiocytes. The taller cylindrical cholangiocytes show mucin production not seen in the small cholangiocytes. Currently, the anatomical-based tumor classification is often problematic due to the three-dimensional biliary structure and large tumor size. We hypothesized that CCs may reflect the heterogeneity of the cholangiocytes and that this may be useful for more precise tumor classification, as tumor histopathology reflects cellular origin. Therefore, we investigated the histological variation in ICCs and compared their different phenotypes with hilar CCs (so-called Klatskin tumor) and CLCs (thought to be originated from HPCs).

We were able to histopathologically categorize ICCs into two groups based on histological diversity; pure muc-ICC and mixed-ICC (mucin-producing adenocarcinoma with hepatocytic differentiation [hep-dif] areas and/or ductular areas). Muc-ICCs had similar clinicopathological, immunohistochemical, and gene expression profiles to hilar CCs, and the tumors had a similar profile to cylindrical, taller, mucin-producing cholangiocytes that line hilar and intrahepatic large BDs. In contrast, mixed-ICCs showed similar clinicopathological, immunohistochemical, and gene

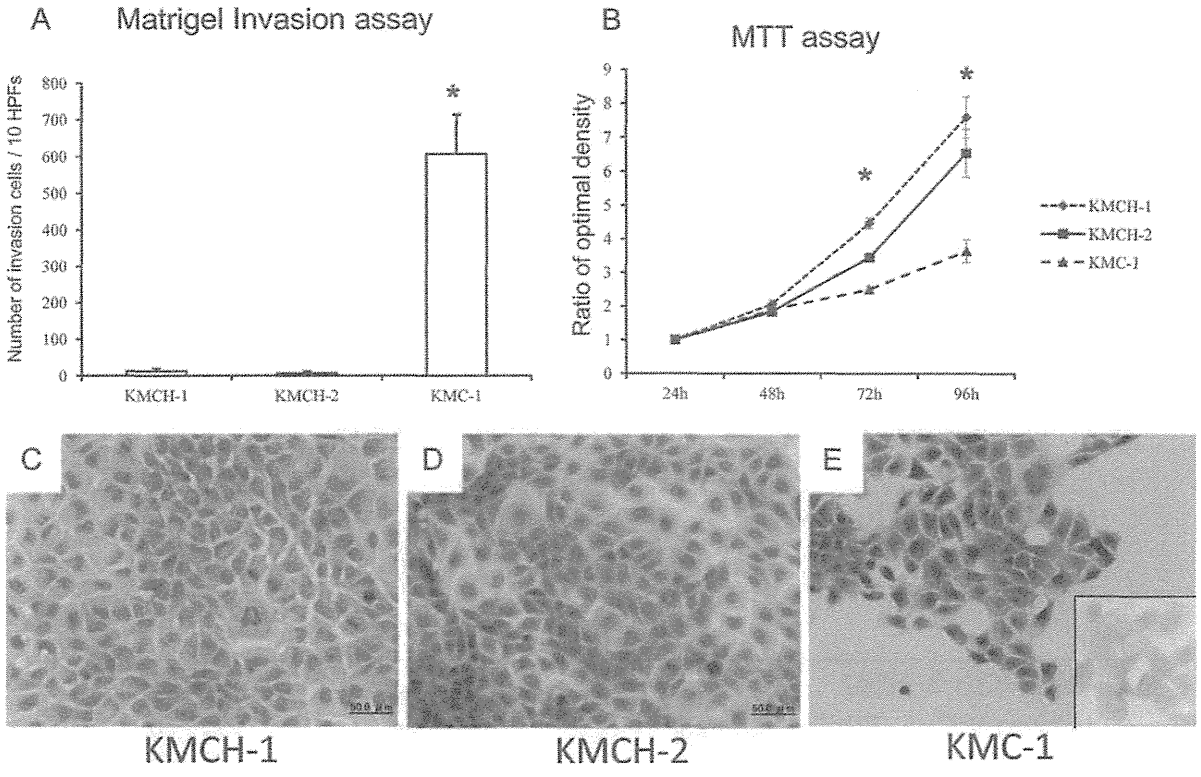

Fig. 5. Invasion and MTT assay. (A) KMC-1 showed significantly higher invasiveness compared with KMCH-1 and KMCH-2. *$P < 0.01$. (B) KMCH-1 and KMCH-2 cells showed a significantly faster proliferation rate at 72 hours and 96 hours compared with KMC-1. *$P < 0.001$. (C) KMCH-1 cells proliferated in pavestone arrangements, showing an abundant eosinophilic cytoplasm with a large, round nucleus containing distinct nucleoli. Some cells revealed cytoplasmic vacuoles. (D) KMCH-2 cells also proliferated with a pavestone arrangement. They comprised two different types of cells: large cells showing abundant eosinophilic cytoplasm with a round nucleus containing distinct nucleoli, and smaller cells with an increased nuclear/cytoplasmic ratio showing dark eosinophilic cytoplasm and oval-shaped, dense nuclei. (E) KMC-1 cells proliferated in a pavement-like monolayer pattern with a partly tubular formation. They had an irregular-shaped, medium to large cytoplasm with irregular-shaped, dark nuclei. Alcian blue-positive mucin was seen (inset).

expression profiles to CLCs (90% ductular areas with focal hep-dif areas and/or mucin-producing CC areas, which are thought to originate from HPCs). These tumors had similar profiles to mucin-negative cuboidal cholangiocytes that line the smallest BD (ductules). These features may indicate their different cells of origin; hilar CCs and muc-ICCs are from the hilar and large intrahepatic BD lined with mucin-producing cholangiocytes, while mixed-ICCs and CLCs are from the most peripheral biliary branches, ductules, which contain HPCs. In that respect, we think that mixed-ICCs and CLCs form part of a spectrum with combined hepatocellular-cholangiocarcinoma, which are also thought to be of possible HPC origin.[18-20]

Histological variation such as hep-dif and ductular areas could be indeed a sign of a HPC-related intrahepatic tumor. Because HPCs are able to differentiate into either hepatocytes or cholangiocytes, HPC-related tumors can display a whole spectrum of phenotypes with varying hepatocellular and cholangiocellular differentiation characteristics.[4,21] In addition, HPCs are located in the most peripheral biliary branches within the liver, so that histological diversity is not seen in the CC originating from the extrahepatic BD, as with hilar CCs. Recognizing these mixed features may be much easier by combining histopathology with immunohistochemistry of markers like NCAM and S100P. S100P, a member of the S100 family of EF-hand calcium-binding proteins,[22] was recently reported to be a useful diagnostic marker of ICC.[9,23] We showed S100P expression in hilar CCs and muc-ICCs only, but not in the mucin-producing adenocarcinoma component of mixed-ICCs. In contrast, NCAM, a marker of HPCs, was only immunoreactive in the hep-dif and ductular areas in mixed-ICCs and CLCs, but not in muc-ICCs and hilar CCs, as reported.[24] These mirror images are useful to distinguish muc-ICCs from mixed-ICCs and CLCs. Gene expression profiling in the different types of CCs showed significant differences in several genes. However, the differences of mRNA level

A

T2-weighted imaging	Homogeneous intensity	Heterogeneous Intensity
	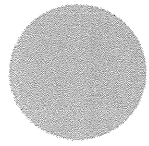	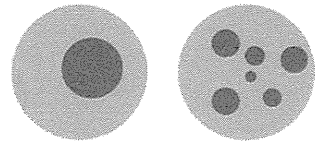
Tumor Type		
Muc-ICC (n=14)	14 (100 %)	0 (0 %)
Mixed-ICC (n=10)	3 (30 %)	7 (70 %)
CLC (n=14)	2 (14 %)	12 (86 %)

B

Tumor type: n (%)	Dynamic series		
	Arterial phase	Portal phase	Venous phase
Muc-ICC: 14 (100 %) Mixed-ICC: 0 (0 %) CLC: 3 (21 %)	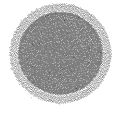 Peripheral enhancement	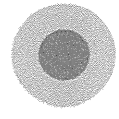 Concentric filling	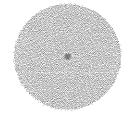 Concentric filling
Muc-ICC: 0 (0 %) Mixed-ICC: 5 (50 %) CLC: 5 (36 %)	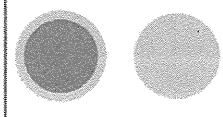 Peripheral or diffuse enhancement	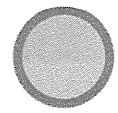 Peripheral wash-out and central enhancement	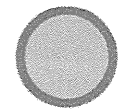 Peripheral wash-out and central enhancement
Muc-ICC: 0 (0 %) Mixed-ICC: 2 (20 %) CLC: 1 (7 %)	 Diffuse enhancement	 Diffuse enhancement	 Diffuse enhancement
Muc-ICC: 0 (0 %) Mixed-ICC: 3 (30 %) CLC: 5 (36 %)	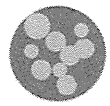 Nodular enhancement	 Nodular pattern of wash-out	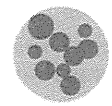 Nodular pattern of wash-out

Fig. 6. Preoperative MRI: lesion characteristics. (A) Schematic representation of the different T2-weighted signal patterns in correlation to the tumor subtypes. (B) Schematic representation of the different contrast-enhancement patterns in correlation to the tumor subtypes.

assessment do not always correlate with the protein levels presented by immunohistochemistry. For instance, *KRT19* and *EpCAM* showed significant up-regulation in muc-ICCs compared with hilar CCs, although their immunoprofiles were exactly the same. Therefore, and for the usefulness of immunohistochemistry in clinical practice, S100P and NCAM are more useful markers.

The histological classification in this study was partially supported by tumor location. The mixed-ICCs and CLCs were mostly located in the periphery of the liver, which mainly comprises smaller BDs, whereas hilar CCs and muc-ICCs were mainly located in the liver hilum, which is predominantly composed of large BD. However, 20%-25% of mixed-ICCs and CLCs were located in the perihilar area, indicating the advantage of the histological-based classification over the anatomically based classification. The finer ramifications (ductules and canals of Hering) are also represented in the (peri-) hilar zones. This highlights the issue of the three-dimensional tree-like structure of the intrahepatic biliary system and the problems associated with the current anatomical-based classification. A

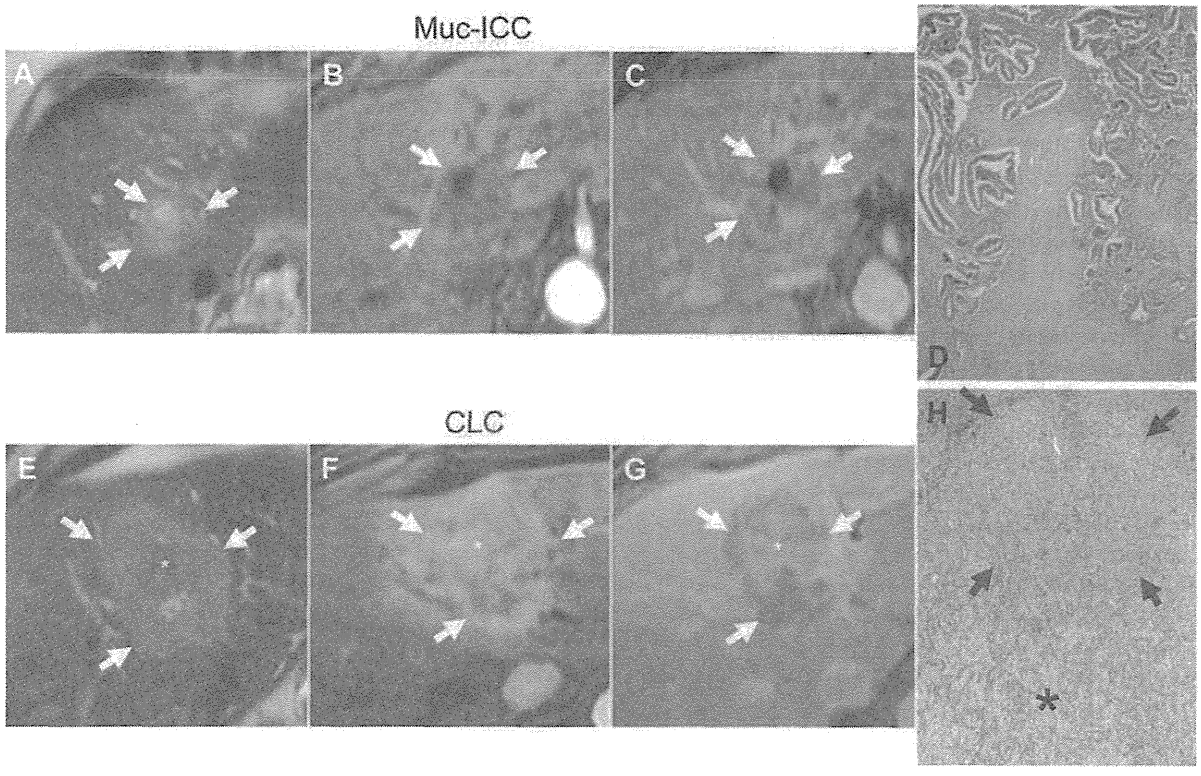

Fig. 7. Historadiological comparison between muc-ICC and CLC. (A) T2-weighted imaging shows homogeneous, moderately hyperintense lesion (arrows) with small necrotic focus. (B) In the arterial phase, the lesion shows moderate peripheral enhancement followed by (C) progressive contrast filling in the venous phase. (D) Muc-ICC showing abundant dense fibrous stroma. (E) T2-weighted imaging shows mixed intensity (peripheral, moderately hyperintense [arrows] and central hypointense [asterisk]). (F) In the arterial phase, the lesion shows heterogeneous, strong arterial enhancement followed by (G) progressive washout in the periphery of the tumor (arrows) and delayed enhancement in the center of the tumor (asterisk). (H) CLC showing hepatocytic differentiation area located in the tumor periphery (arrows) and ductular area located in the tumor center (asterisk).

further advantage was highlighted when we were able to classify the ICCs, even in large ICCs (mixed-ICC, 67.3 mm; CLC, 64.6 mm; muc-ICC, 41.2 mm); estimating the origin of the tumor using the current anatomical tumor classification becomes more problematic with increasing tumor size. These findings favor the proposed histological classification as a more accurate representative, reliable, and simple approach compared with anatomical classification.

Clinicopathological features differed in hilar CCs and muc-ICCs, compared with mixed-ICCs and CLCs. Mixed-ICCs and CLCs showed mostly a peripheral location, larger tumor size, less lymphatic invasion, and less perineural invasion. In contrast, hilar CCs and muc-CCs showed mostly a hilar location, smaller tumor size, more lymphatic invasion, and more perineural invasion. Immunohistochemically, the expression of S100P and cytoplasmic MUC1, reportedly prognostic markers for poor outcome in CCs[25,26] and other cancers,[27,28] was seen only in hilar CCs and muc-ICCs. In addition, TACSTD2 overexpression, reportedly an independent prognostic marker of poor outcome in several human carcinomas,[14,29] was more frequently seen in hilar CCs and muc-ICCs. This would suggest that hilar CCs and muc-ICCs are more aggressive when compared with mixed-ICCs and CLCs. This was supported by our *in vitro* data where the cell line corresponding to muc-ICCs had a significantly higher invasiveness compared with those corresponding to mixed-ICCs. The data indicate a clinical requirement to identify muc-ICCs from the other subtypes of CCs. Nonetheless, our data did not reveal a significantly different prognosis between the four groups, although the hilar CCs and muc-ICCs group tended to show worse prognosis compared with the mixed-ICCs and CLCs group. This may be due to the difference in the time of diagnosis in hilar CCs and muc-ICCs relative to mixed-CCs and CLCs. Because hilar CCs and muc-ICCs are mainly located in the liver hilum (associated with biliary problems), they can

be detected earlier when the tumor is smaller. This is also supported by the fact that the mixed-ICCs and CLCs tended to show larger tumor size and several nodules compared with hilar CCs and muc-ICCs. However, further investigation on the prognostic impact of mixed-CCs and CLCs in a larger study group is required.

In our series, one hilar CC and one mixed-ICC were diagnosed in the explanted liver. Hilar CC was found in a patient with PSC and with hilar BD stenosis, and the tumor was a periductal infiltrating type with moderately differentiated adenocarcinoma. A mixed-ICC of the mass-forming type and containing both hep-dif and ductular areas in the tumor was detected in a patient with hepatitis B– and C–related liver cirrhosis. Preoperative imaging of this ICC showed partial mimicking of a HCC-like pattern, such as early enhancement in the arterial phase and washout in the portal phase, and it was diagnosed as HCC and proceeded into liver transplantation without histological examination. Because ICC often shows lymph node metastasis (compared with HCC), it is not an indication for liver transplantation. However, in our series, all mixed-ICCs and CLCs showed mass-forming growth patterns and contained hep-dif areas in the tumor; these features may mimic HCC features in preoperative imaging. Mimicking of the HCC pattern has been reported with imaging in CLCs[30] and CCs.[31] In addition, our MRI data showed overlapping imaging characteristics between mixed-ICCs and CLCs. Therefore, histological assessment could be considered in patients who are hepatitis virus–positive and have a tumor with an atypical HCC pattern in preoperative examination.

To identify mixed features by preoperative needle biopsy, we studied five preoperative needle biopsies with a postoperative diagnosis of muc-ICC (n = 1) and mixed-ICC (n = 4). Three of the four mixed-ICCs were correctly diagnosed because they contained hep-dif or ductular areas together with a mucin-producing adenocarcinoma area. However, one biopsy was diagnosed as muc-ICC because the tumor sample contained only a mucin-producing adenocarcinoma area. We therefore conclude that if mixed features are detected in the biopsy, a mixed-ICC diagnosis can be made; however, the opposite is not always true.

In conclusion, about 39% of the ICCs studied presented with mixed features (hep-dif and ductular areas [mixed-ICCs]), whereas the remaining ICCs showed pure mucin-producing CCs (muc-ICCs). Mixed-ICCs showed similar clinicopathological, immunohistochemical, and gene expression profiles to CLCs (thought to be of HPC origin), and the immunohistochemical and gene expression profiles were similar to the most peripheral bile ductules. In contrast, muc-ICCs showed a similar profile to hilar CCs (so-called Klatskin tumor), and those profiles were similar to the mucin-producing cholangiocytes that line the hilar BD and intrahepatic large BD. These features probably reflect the different cell of origin. Histological classification may help in resolving the issues of current anatomical-based and pathological classification of CC. The immunoreactivity of S100P and NCAM represents a useful tool to distinguish mixed-ICC from muc-ICC.

References

1. Desmet V, Roskams T, Vos RD. Normal anatomy. In: Feldman M, ed. Gastroenterology and Hepatology. The Comprehensive Visual Reference. Philadelphia, PA: Current Medicine, Inc.; 1997:1.14.
2. Roskams TA, Theise ND, Balabaud C, Bhagat G, Bhathal PS, Bioulac-Sage P, et al. Nomenclature of the finer branches of the biliary tree: canals, ductules, and ductular reactions in human livers. HEPATOLOGY 2004;39:1739-1745.
3. Roskams T, Katoonizadeh A, Komuta M. Hepatic progenitor cells: an update. Clin Liver Dis 2010;14:705-718.
4. Komuta M, Spee B, Vander Borght S, De Vos R, Verslype C, Aerts R, et al. Clinicopathological study on cholangiolocellular carcinoma suggesting hepatic progenitor cell origin. HEPATOLOGY 2008;47: 1544-1556.
5. Nakanuma Y, Curado M-P, Franceschi S, Gores G, Paradis V, Sripa B, et al. Intrahepatic cholangiocarcinoma. Lyon, France: IARC; 2010.
6. Edge SB, Byrd DR, Compton CC, Fritz AG, Greene FL, Trotti III A. Perihilar Bile Ducts. 7th ed. Chicago, IL: Springer; 2010.
7. Han JK, Choi BI, Kim AY, An SK, Lee JW, Kim TK, et al. Cholangiocarcinoma: pictorial essay of CT and cholangiographic findings. Radiographics 2002;22:173-187.
8. Liver Cancer Study Group of Japan. Classification of Primary Liver Cancer. 1st English ed. Tokyo, Japan: Kanehara; 1997.
9. Levy M, Lin F, Xu H, Dhall D, Spaulding BO, Wang HL. S100P, von Hippel-Lindau gene product, and IMP3 serve as a useful immunohistochemical panel in the diagnosis of adenocarcinoma on endoscopic bile duct biopsy. Hum Pathol 2010;41:1210-1219.
10. Roskams T, De Vos R, Van Eyken P, Myazaki H, Van Damme B, Desmet V. Hepatic OV-6 expression in human liver disease and rat experiments: evidence for hepatic progenitor cells in man. J Hepatol 1998;29:455-463.
11. Okabe M, Tsukahara Y, Tanaka M, Suzuki K, Saito S, Kamiya Y, et al. Potential hepatic stem cells reside in EpCAM+ cells of normal and injured mouse liver. Development 2009;136:1951-1960.
12. Schmelzer E, Zhang L, Bruce A, Wauthier E, Ludlow J, Yao HL, et al. Human hepatic stem cells from fetal and postnatal donors. J Exp Med 2007;204:1973-1987.
13. Jozefczuk J, Stachelscheid H, Chavez L, Herwig R, Lehrach H, Zeilinger K, et al. Molecular characterization of cultured adult human liver progenitor cells. Tissue Eng Part C Methods 2010;16:821-834.
14. Fong D, Moser P, Krammel C, Gostner JM, Margreiter R, Mitterer M, et al. High expression of TROP2 correlates with poor prognosis in pancreatic cancer. Br J Cancer 2008;99:1290-1295.
15. Iemura A, Maruiwa M, Yano H, Kojiro M. A new human cholangiocellular carcinoma cell line (KMC-1). J Hepatol 1992;15:288-298.
16. Murakami T, Yano H, Maruiwa M, Sugihara S, Kojiro M. Establishment and characterization of a human combined hepatocholangiocarcinoma cell line and its heterologous transplantation in nude mice. HEPATOLOGY 1987;7:551-556.

17. Yano H, Iemura A, Haramaki M, Momosaki S, Ogasawara S, Higaki K, et al. A human combined hepatocellular and cholangiocarcinoma cell line (KMCH-2) that shows the features of hepatocellular carcinoma or cholangiocarcinoma under different growth conditions. J Hepatol 1996;24:413-422.
18. Theise ND, Yao JL, Harada K, Hytiroglou P, Portmann B, Thung SN, et al. Hepatic 'stem cell' malignancies in adults: four cases. Histopathology 2003;43:263-271.
19. Kim H, Park C, Han KH, Choi J, Kim YB, Kim JK, et al. Primary liver carcinoma of intermediate (hepatocyte-cholangiocyte) phenotype. J Hepatol 2004;40:298-304.
20. Roskams T. Anatomic pathology of hepatocellular carcinoma: impact on prognosis and response to therapy 2011. Clin Liver Dis;15: 245-259.
21. Roskams T. Liver stem cells and their implication in hepatocellular and cholangiocarcinoma. Oncogene 2006;25:3818-3822.
22. Donato R. S100: a multigenic family of calcium-modulated proteins of the EF-hand type with intracellular and extracellular functional roles. Int J Biochem Cell Biol 2001;33:637-668.
23. Hamada S, Satoh K, Hirota M, Kanno A, Ishida K, Umino J, et al. Calcium-binding protein S100P is a novel diagnostic marker of cholangiocarcinoma. Cancer Sci 2011;102:150-156.
24. Gutgemann I, Haas S, Berg JP, Zhou H, Buttner R, Fischer HP. CD56 expression aids in the differential diagnosis of cholangiocarcinomas and benign cholangiocellular lesions. Virchows Arch 2006;448:407-411.
25. Aishima S, Fujita N, Mano Y, Kubo Y, Tanaka Y, Taketomi A, et al. Different roles of S100P Overexpression in Intrahepatic Cholangiocarcinoma: Carcinogenesis of Perihilar Type and Aggressive Behavior of Peripheral Type. Am J Surg Pathol 2011;35:590-598.
26. Matsumura N, Yamamoto M, Aruga A, Takasaki K, Nakano M. Correlation between expression of MUC1 core protein and outcome after surgery in mass-forming intrahepatic cholangiocarcinoma. Cancer 2002;94:1770-1776.
27. Wang G, Platt-Higgins A, Carroll J, de Silva Rudland S, Winstanley J, Barraclough R, et al. Induction of metastasis by S100P in a rat mammary model and its association with poor survival of breast cancer patients. Cancer Res 2006;66:1199-1207.
28. van der Vegt B, de Roos MA, Peterse JL, Patriarca C, Hilkens J, de Bock GH, et al. The expression pattern of MUC1 (EMA) is related to tumour characteristics and clinical outcome of invasive ductal breast carcinoma. Histopathology 2007;51:322-335.
29. Muhlmann G, Spizzo G, Gostner J, Zitt M, Maier H, Moser P, et al. TROP2 expression as prognostic marker for gastric carcinoma. J Clin Pathol 2009;62:152-158.
30. Asayama Y, Tajima T, Okamoto D, Nishie A, Ishigami K, Ushijima Y, et al. Imaging of cholangiolocellular carcinoma of the liver. Eur J Radiol 2010;75:e120-e125.
31. Rimola J, Forner A, Reig M, Vilana R, de Lope CR, Ayuso C, et al. Cholangiocarcinoma in cirrhosis: absence of contrast washout in delayed phases by magnetic resonance imaging avoids misdiagnosis of hepatocellular carcinoma. HEPATOLOGY 2009;50:791-798.

Published OnlineFirst May 18, 2012; DOI:10.1158/1078-0432.CCR-11-2041

Clinical Cancer Research

Vandetanib, an Inhibitor of VEGF Receptor-2 and EGF Receptor, Suppresses Tumor Development and Improves Prognosis of Liver Cancer in Mice

Kinya Inoue[1], Takuji Torimura[1,3], Toru Nakamura[1], Hideki Iwamoto[1], Hiroshi Masuda[1], Mitsuhiko Abe[1], Osamu Hashimoto[1], Hironori Koga[1], Takato Ueno[1], Hirohisa Yano[2], and Michio Sata[1,3]

Abstract

Purpose: VEGF, EGF, and TGF-α are expressed in hepatocellular carcinomas (HCC) and play a role in its growth. Vandetanib, a multikinase inhibitor, suppresses the phosphorylation of VEGF receptor 2 (VEGFR-2) and EGF receptor (EGFR). The aim of this study was to clarify the antitumor effect of vandetanib in mouse HCCs.

Experimental Design: We evaluated the effects of vandetanib on proliferation of human umbilical vein endothelial cells (HUVEC) and three hepatoma cell lines, as well as the phosphorylation of VEGFR-2 and EGFR in these cells. Mice were implanted with hepatoma cells subcutaneously or orthotopically in the liver and treated with 50 or 75 mg/kg vandetanib. We analyzed the effects of treatment on tumor cell proliferation and apoptosis, vessel density, phosphorylation of VEGFR-2 and EGFR, and production of VEGF, TGF-α, and EGF in tumor tissues. Adverse events on vandetanib administration were also investigated.

Results: Vandetanib suppressed phosphorylation of VEGFR-2 in HUVECs and EGFR in hepatoma cells and inhibited cell proliferation. In tumor-bearing mice, vandetanib suppressed phosphorylation of VEGFR-2 and EGFR in tumor tissues, significantly reduced tumor vessel density, enhanced tumor cell apoptosis, suppressed tumor growth, improved survival, reduced number of intrahepatic metastases, and upregulated VEGF, TGF-α, and EGF in tumor tissues. Treatment with vandetanib was not associated with serious adverse events, including alanine aminotransferase abnormality, bone marrow suppression, or body weight loss.

Conclusions: The antitumor effects of vandetanib in mice suggest that it is a potentially suitable and safe chemotherapeutic agent for HCCs. *Clin Cancer Res; 18(14); 3924–33. ©2012 AACR.*

Introduction

Hepatocellular carcinoma (HCC) is one of the most common malignant tumors in the tropics and the Far East, including Japan (1). Recently, in the SHARP trial, a phase III, randomized, placebo-controlled trial established the efficacy of sorafenib, a multikinase inhibitor, in patients with advanced HCCs (2, 3). It is known to suppress the activities of the Raf/mitogen-activated protein kinase/extracellular signal–regulated kinase (Raf/MEK/ERK) signaling pathway, tyrosine kinase VEGF receptor (VEGFR)-2, VEGFR-3, and platelet-derived growth factor receptor-β (PDGFR-β), in patients with advanced HCCs (4–6). However, the benefits of sorafenib are limited to prolongation of survival for only 3 months. Thus, other molecular target agents are required for the treatment of advanced HCCs.

Tumor growth and formation of metastases are dependent on the existence of adequate blood supply (7, 8).

In HCCs, the tumor tissue is supplied by blood from new arteries and the development of rich vasculature occurs in parallel with tumor development (9). VEGF plays a critical role in the process of angiogenesis (10, 11). VEGF is produced by hepatoma cells, hepatic stellate cells, and endothelial cells, and its expression level correlates with tumor growth (12). Hepatoma cells also produce EGF and TGF-α and express EGF receptor (EGFR; ref. 13). Increasing evidence has highlighted the importance of EGFR and its ligands EGF and TGF-α in hepatocarcinogenesis (14, 15).

Vandetanib (Zactima; ZD6474) is an orally bioavailable, small-molecule VEGFR-tyrosine kinase inhibitor with additional activity against EGFR-tyrosine kinase and RET receptor tyrosine kinase (16). Therefore, vandetanib, in addition to inhibiting endothelial cell proliferation through the

Authors' Affiliations: [1]Division of Gastroenterology, Department of Medicine, [2]Department of Pathology, Kurume University School of Medicine, and [3]Liver Cancer Division, Research Center for Innovative Cancer Therapy, Kurume University, Fukuoka, Japan

Note: Supplementary data for this article are available at Clinical Cancer Research Online (http://clincancerres.aacrjournals.org/).

Corresponding Author: Takuji Torimura, Liver Cancer Division, Research Center for Innovative Cancer Therapy, Kurume University, 67 Asahi-machi, Kurume City, Fukuoka 830-0011, Japan. Phone: 81-942-317746; Fax: 81-942-317747l; E-mail: tori@med.kurume-u.ac.jp

doi: 10.1158/1078-0432.CCR-11-2041

Published OnlineFirst May 18, 2012; DOI:10.1158/1078-0432.CCR-11-2041

Translational Relevance

VEGF plays the significant role of vascular development in hepatocellular carcinomas (HCC). Recently, several clinical trials of molecular-targeted agents for advanced HCCs have been investigated. On the basis of their results, it has been proved that antiangiogenic agents such as sorafenib are effective for advanced HCCs. However, their efficacies are not fully satisfied yet. EGF receptor signaling is upregulated in HCCs. Vandetanib, a multi-tyrosine kinase inhibitor, is known to suppress the phosphorylation of EGF receptor and VEGF receptor-2 (VEGFR-2). Here, we show for the first time that vandetanib suppressed tumor growth, intrahepatic metastasis and prolonged the survival of mouse HCC model and that these effects are mainly mediated by inhibition of vascular formation. In addition, vandetanib was effective for enlarged mouse HCC model. These preclinical results suggest that vandetanib could be potentially useful for patients with advanced HCCs.

blockade of VEGF-induced signaling, can suppress tumor cell growth more directly through the blockade of EGFR autocrine signaling (17).

The present study was designed to assess the antitumor effects and adverse effects of vandetanib in mouse HCC models.

Materials and Methods

Reagents, cells, and animals

We used 3 hepatoma cell lines, HAK1-B, HuH-7, and KYN-2. Human umbilical vein endothelial cells (HUVEC) and HuH-7 were obtained from CAMBREX Bio Science Walkersville Inc. KYN-2 (18) and HAK1-B (19) were obtained from the Department of Pathology of our university. Male 5-week-old nude mice (BALB/c *nu/nu*; Kyudo KK.) and mice with severe-combined immunodeficiency (SCID; CB-7/1cr, Kyudo KK.) were acclimatized and placed in separate cages. All animals received humane care according to the guideline of the NIH for the Policy on Humane Care and Use of Laboratory Animals. The experimental protocol was approved by the Laboratory Animal Care and Use Committee of Kurume University (Fukuoka, Japan).

In vitro inhibition of cell proliferation by vandetanib

Approximately 1,000 HUVECs in 200 μL of endothelial cell growth medium-2 (EGM-2) medium (EGM-2 Bullet Kit; Clonetics) supplemented with 5% FBS were added to each well of 96-well plastic dishes and incubated at 37°C for 24 hours. The medium was replaced with 200 μL of EBM-2 with 5% FBS containing various concentrations of vandetanib (0, 0.01, 0.05, 0.1, 0.5, 1.0, 10.0 μmol/L). After incubation for 30 minutes, VEGF (3 ng/mL) was added. In another experiment, approximately 1,000 hepatoma cells in 200 μL of Dulbecco's Modified Eagle's Medium (DMEM; Gibco Invitrogen Cell Culture) supplemented with 10% FBS were added to each well of 96-well plastic dishes and incubated at 37°C for 24 hours. The medium was replaced with 200 μL of medium containing various concentrations of vandetanib (0, 0.05, 0.1, 0.5, 1.0, 5.0, 10.0 μmol/L). After incubation for 72 hours, cell proliferation was measured by a tetrazolium-based assay (Cell Count Reagent SF; Nacalai Tesque Inc.). Then, we conducted cell-cycle analysis of 3 hepatoma cell lines by flow cytometry. After incubation for 72 hours with vandetanib (0, 10 μmol/L), the floating and attached cells were harvested and washed with PBS. The DNA content was assessed by staining ethanol-fixed cells with propidium iodide and monitoring by FACSCalibur (Becton Dickinson). The percentage of cells in the sub-G_0/G_1 population was determined using CellQuest software (BD).

Western blotting

HUVECs were cultured in serum-free and VEGF-free medium, and hepatoma cells were cultured in serum-free medium for 12 hours. HUVECs were treated with various concentrations of vandetanib (0, 1.0, 5.0, 10.0 μmol/L) for 60 minutes and then incubated with VEGF (0, 50 ng/mL) for 5 minutes. Hepatoma cells were treated with vandetanib (0, 1.0, 5.0, 10.0 μmol/L) for 60 minutes and then incubated with EGF (0, 100 ng/mL) for 5 minutes. Total cell protein (50 μg) and tissue lysates were run on 10% SDS-PAGE and transferred to polyvinylidene difluoride membranes. The membranes were incubated overnight at 4°C with rabbit anti-phosphorylated VEGFR-2 antibody (Ty1175; Cell Signaling Technology Inc.), rabbit anti-VEGFR-2 antibody (Calbiochem-Novabiochem Corporation), rabbit anti-phosphorylated EGFR (Ty1173; Cell Signaling Technology Inc.), rabbit anti-EGFR (Cell Signaling Technology), rabbit anti-VEGF antibody (Abcam Japan), rat anti-EGF antibody (Monosan), rabbit anti-TGF-α antibody (Abcam Japan), and mouse anti-actin antibody (Sigma-Aldrich, Inc.). Each antibody was diluted 500-fold. After incubation with secondary donkey anti-rabbit horseradish peroxidase (HRP)-conjugated IgG (dilution, 1:10,000 dilution; GE Healthcare Bio-Sciences GK), anti-rat HRP-conjugated mouse IgM (dilution, 1:2,000; Zymed Laboratories), or donkey anti-mouse HRP-conjugated IgG (dilution, 1:5,000; GE Healthcare Bio-Sciences GK) for 1 hour, immunoreactive bands were stained by an enhanced chemiluminescence Western blot analysis system (Amersham Pharmacia Biotech).

Protocols of tumor growth studies of subcutaneous tumor models

Tumor cells (5×10^6) were injected subcutaneously into the dorsal side in nude mice. The tumor-bearing mice were randomly divided into PBS-treated group ($n = 6$) and vandetanib-treated groups ($n = 6$). Treatment was initiated when the average size of the tumor reached 50 to 100 mm^3; the tumor-bearing mice were orally administered PBS or vandetanib (50 or 75 mg/kg) every day. To evaluate the

Published OnlineFirst May 18, 2012; DOI:10.1158/1078-0432.CCR-11-2041

antitumor effect of vandetanib in mice bearing large tumors of HuH-7 (>500 mm^3), the mice received PBS ($n = 6$) or vandetanib (75 mg/kg; $n = 6$). Two dimensions of the tumor were measured by calipers every 3 days, and the tumor volume was calculated by the equation: length × $width^2 \times 0.52$.

Protocols of growth, survival, and intrahepatic metastases studies of liver tumor models

For tumor growth studies, nude mice were injected with KYN-2 into the liver. The mice were randomly divided into PBS-treated group ($n = 6$) and vandetanib-treated groups (50 mg/kg, $n = 6$; 75 mg/kg, $n = 6$). After 7 days, the mice were treated orally with vandetanib every day for 3 weeks. They were subsequently sacrificed at day 28, and tumor volume was evaluated.

For survival studies, KYN-2 cells were implanted into another group of 12 nude mice, which were then randomly divided into PBS-treated group ($n = 6$) and vandetanib-treated group (75 mg/kg; $n = 6$). Mice were sacrificed according to the clinical signs of weakness, anorexia, or more than 20% weight loss.

To evaluate intrahepatic metastasis, 2×10^6 KYN-2 cells were implanted into the liver of SCID mice. The mice were then randomly divided into PBS-treated group ($n = 6$) and vandetanib-treated group (75 mg/kg; $n = 6$). Administration of vandetanib for 3 weeks was followed by counting the number of intrahepatic nodules.

Assessment of vascular density, proliferation activity, and apoptotic index in tumor tissues of liver tumor model

The sections of liver tumor tissues were incubated with rabbit anti-mouse CD31 antibody (dilution, 1:100; Abcam Japan) and rabbit anti-PCNA antibody (dilution, 1:100; Santa Cruz Biotechnology, Inc.) at 4°C overnight. Then, the sections were incubated with fluorescein isothiocyanate (FITC)-conjugated (dilution, 1:100) or EnVision+System-HRP-labeled polymer anti-rabbit (Dako Japan). The sections were also examined for apoptosis of tumor cells by terminal deoxynucleotidyl transferase–mediated dUTP nick end labeling (TUNEL) staining with In Situ Apoptosis detection kit (Oncor). The numbers of CD31-positive blood vessels in tumor tissues were counted in 50 blindly selected random fields (z-series, ×63 oil magnification). Proliferating cell nuclear antigen (PCNA)- and TUNEL-positive cells among 1,000 hepatoma cells were counted in 28 blindly selected random fields.

Measurement of serum levels of α-fetoprotein, vandetanib, alanine aminotransferase, bone marrow functions, and body weight

Serum α-fetoprotein (AFP) levels were measured at the time of sacrifice in tumor-bearing mice. Serum levels of vandetanib were measured by high-performance liquid chromatography (HPLC) at the time of sacrifice. We also determined leukocyte and platelet counts, hemoglobin (Hb) levels, and serum alanine aminotransferase (ALT) levels. Body weight was evaluated at the start of treatment and at sacrifice.

Statistical analysis

All data were expressed as mean ± SD. Differences between groups were examined for statistical significance using the Mann–Whitney *U* test, the Kruskal–Wallis rank test, and the log-rank test. A *P* value less than 0.05 denoted the presence of a statistically significant difference.

Results

Vandetanib inhibits endothelial cell and hepatoma cell proliferation

Vandetanib suppressed cell proliferation of HUVECs (IC_{50} = 7.1 μmol/L) from 0.01 μmol/L of vandetanib in a dose-dependent manner (Fig. 1A). It also suppressed cell proliferation of the human hepatoma cell line (HAK1-B; IC_{50} = 10.0 μmol/L) in a dose-dependent manner from 0.05 μmol/L of vandetanib (Supplementary Fig. S1A). Vandetanib also suppressed the proliferation of KYN-2 cells (IC_{50} = 8.1 μmol/L) and HuH-7 cells (IC_{50} = 9.4 μmol/L) from 5 to 10 μmol/L of vandetanib (Supplementary Fig. S1B and S1C). The rates of apoptosis of vandetanib-treated hepatoma cells (HAK1-B, 74.3%; KYN-2, 41.8%; HuH-7, 62.5%) were higher than those of nontreated hepatoma cells (HAK1-B, 20.4%; KYN-2, 10.7%; HuH-7, 31.3%; Fig. 1B).

Vandetanib inhibits phosphorylation of VEGFR-2 and EGFR

Vandetanib (at both 5 and 10 μmol/L) significantly inhibited VEGFR-2 phosphorylation in HUVECs (Fig. 1C). Although vandetanib (at 1–10 μmol/L) suppressed EGFR phosphorylation in the 3 hepatoma cell lines (Fig. 1D; Supplementary Fig. S2A and S2B), it did not affect the expression of total VEGFR-2 and EGFR in the same cells.

Vandetanib inhibits tumor growth of hepatoma cells in subcutaneous tumor model

In the HuH-7 xenograft model, the tumor volumes at baseline of the PBS group and 50 and 75 mg/kg vandetanib groups were 63.5 ± 11.9, 70.3 ± 16.2, and 72.3 ± 11.6 mm^3, respectively. After 3 weeks of treatment, the respective tumor volumes were 4,704.7 ± 2,205.4, 773.4 ± 458.5, and 279.4 ± 91.9 mm^3, respectively (Fig. 2A). In another experiment, treatment commenced when tumor volume was more than 500 mm^3. Before treatment, the tumor volumes were 570.0 ± 95.6 mm^3 and 614.5 ± 169.2 mm^3 in the PBS and 75 mg/kg vandetanib groups, respectively. After 15 days of treatment, the respective tumor volumes were 2,491.1 ± 1,451.9 and 572.2 ± 441.5 mm^3 (Fig. 2B).

In the HAK1-B xenograft model, the tumor volumes before treatment of the PBS and 50 mg/kg vandetanib groups were 68.8 ± 12.2 and 75.6 ± 15.4 mm^3, respectively.

Published OnlineFirst May 18, 2012; DOI:10.1158/1078-0432.CCR-11-2041

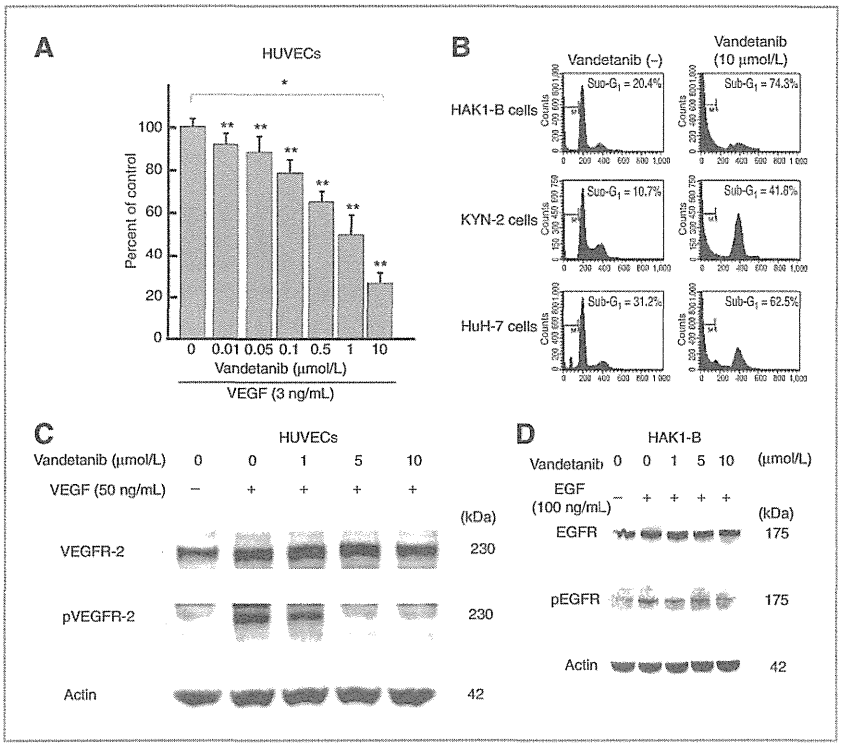

Figure 1. Inhibitory effects of vandetanib on cell proliferation, and phosphorylation of VEGFR-2 and EGFR. A, HUVECs were cultured with a medium containing vandetanib, FBS, and VEGF. Seventy-two hours later, cell proliferation was evaluated by the tetrazolium-based assay. B, hepatoma cells were cultured with a medium containing vandetanib (0, 10 μmol/L) and FBS. Seventy-two hours after incubation, ethanol-fixed floating and attached cells were stained with propidium iodide. Cell apoptosis and cell cycle were determined by flow cytometry. C, HUVECs were cultured in the medium containing vandetanib and VEGF. D, HAK1-B hepatoma cells were cultured in a medium containing vandetanib and EGF. Data are mean ± SD. *, $P < 0.05$, compared with the control by Kruskal–Wallis test; **, $P < 0.05$, compared with the control by Mann–Whitney U test. pEGFR, phosphorylated EGFR; pVEGFR-2, phosphorylated VEGFR-2.

After 3 weeks, the respective tumor volumes were 461.4 ± 134.9 and 169.8 ± 37.8 mm^3 (Fig. 2C). In the KYN-2 xenograft model, the tumor volumes before treatment of the PBS and 50 mg/kg vandetanib groups were 56.7 ± 12.0 and 62.6 ± 13.3 mm^3, respectively, which increased at 3 weeks after the treatment to 10,092.9 ± 7,795.3 and 1,434.4 ± 903.1 mm^3, respectively (Fig. 2D).

Vandetanib inhibits tumor growth and phosphorylation of VEGFR-2 and EGFR

In mice implanted with KYN-2 cells, tumor volume showed a significant inverse relationship with the dose of administered vandetanib (PBS group, 2,137.4 ± 873.3 mm^3; 50 mg/kg vandetanib group, 928.9 ± 515.5 mm^3; 75 mg/kg vandetanib group, 295.5 ± 427.6 mm^3; Fig. 3A; Supplementary Fig. S3A). Serum AFP levels were 50,567 ± 11,300 and 16,540 ± 14,297 ng/mL in the PBS and 75 mg/kg vandetanib groups, respectively (Supplementary Fig. S3B). In tumor-bearing mice treated with vandetanib, tumor tissues showed significant suppression of VEGFR-2 and EGFR phosphorylation (Fig. 3B and C). The production levels of VEGF, TGF-α, and EGF were significantly upregulated in the 50 and 75 mg/kg vandetanib-treated groups compared with the PBS-treated group (Fig. 3D).

Vandetanib prolongs survival of tumor-bearing mice

The survival time ranged from 55 to 75 days (mean, 66.4 ± 8.6 days) in mice bearing tumors of KYN-2 treated with 75 mg/kg vandetanib. This was significantly longer than that of PBS-treated mice (range, 28–62 days; mean, 40.5 ± 11.7 days; Fig. 4A). However, all tumor-bearing mice ultimately died of tumor growth.

Vandetanib inhibits intrahepatic tumor metastasis

In the PBS group, the number of tumor nodules in livers implanted with KYN-2 cells ranged from 4 to 16 (mean, 7.7 ± 4.5). Treatment with 75 mg/kg vandetanib significantly reduced the number of tumor nodules (range, 3–4; mean, 3.2 ± 0.4; Fig. 4B).

Serum vandetanib levels and inhibition of tumor vascularization

Serum vandetanib levels in mice treated with 50 and 75 mg/kg ranged from 2.5 to 14.1 μmol/L (mean, 7.3 ± 4.6)

Published OnlineFirst May 18, 2012; DOI:10.1158/1078-0432.CCR-11-2041

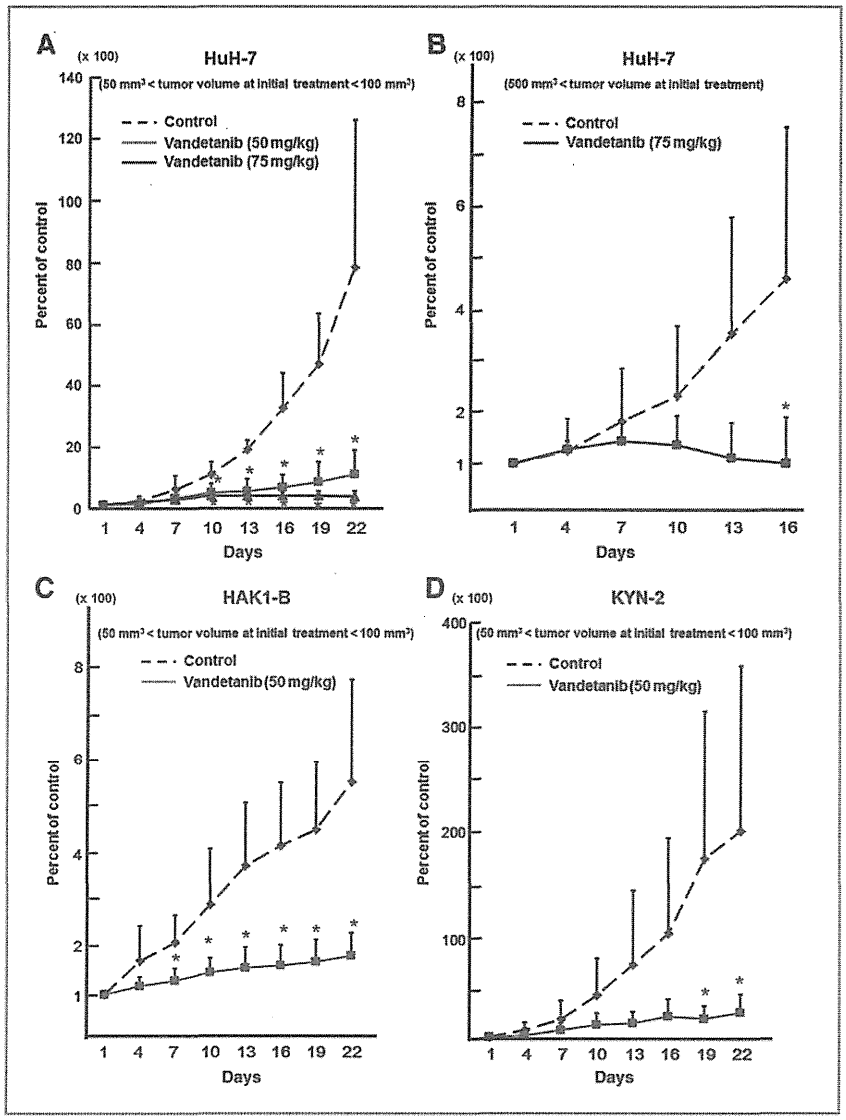

Figure 2. Serial changes in tumor growth induced by treatment with vandetanib in mice carrying subcutaneously implanted human hepatoma cell tumors. Mean ± SD tumor volume is expressed as percentage of the control ($n = 6$ per group). A, HuH-7 cells: treatment commenced when tumor volume was 50 to 100 mm^3. *, $P < 0.05$, compared with PBS-treated mice by Mann–Whitney U test. B, HuH-7: treatment commenced when tumor volume was more than 500 mm^3 to evaluate antitumor effect of vandetanib on enlarge tumors. *, $P < 0.05$, compared with PBS-treated mice by Mann–Whitney U test. (C) HAK1-B and (D) KYN-2: treatment commenced when tumor was 50 to 100 mm^3. *, $P < 0.05$, compared with PBS-treated mice by Mann–Whitney U test.

and 3.8 to 12.7 μmol/L (mean, 8.5 ± 3.0) at the time of sacrifice, respectively. The mean number of vessels in tumor tissues of the PBS, 50 and 75 mg/kg vandetanib groups were 15.6 ± 7.4 per high-power field (HPF), 9.3 ± 2.9 per HPF, and 6.0 ± 2.4 per HPF, respectively. Vandetanib suppressed vascular development in a dose-dependent manner (Fig. 5A and B). The vascular density in these tumors correlated with tumor volume (data not shown).

Effects of vandetanib on cell proliferation and apoptosis in tumor tissues

Vandetanib had not effect on cell proliferation of hepatoma cells (data not shown), but it increased the apoptotic index in tumor tissues from 1.2% ± 0.7% in the PBS to 2.5% ± 0.7% and 3.1% ± 0.9% in the 50 and 75 mg/kg treatment groups, respectively. The effect of vandetanib on apoptosis was dose-dependent.

Effects of vandetanib on serum ALT, body weight, and bone marrow function

There was no significant difference in body weight between the start and end of treatment in the PBS group, 50, and 75 mg/kg vandetanib groups. There were also no significant differences in body weight of the 3 groups at the start of treatment and at sacrifice (Fig. 6A). There were also no significant differences of serum ALT levels, leukocyte count, platelet count, and Hb levels among the 3 groups at sacrifice (Fig. 6B and C).

Published OnlineFirst May 18, 2012; DOI:10.1158/1078-0432.CCR-11-2041

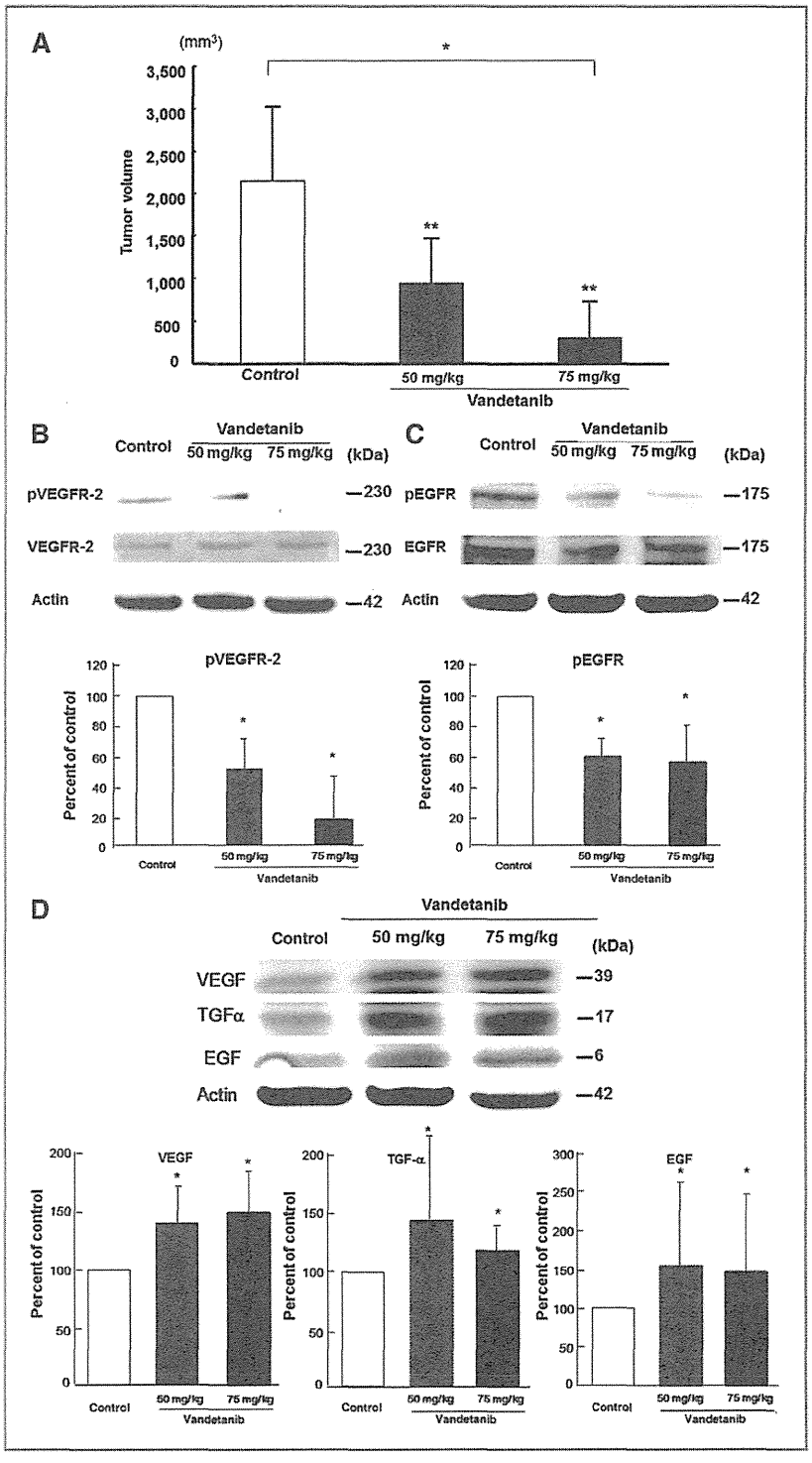

Figure 3. Vandetanib inhibits tumor growth in the liver in nude mice. A, comparison of tumor volume. Tumor volumes are expressed as mean ± SD ($n = 6$ per group). *, $P < 0.05$, by Kruskal-Wallis test; **, $P < 0.05$, by Mann–Whitney U test compared with PBS-treated mice. B, expression of pVEGFR-2 and VEGFR-2. C, Expression of pEGFR and EGFR. D, expression of VEGF, TGF-α, and EGF. Tissue lysate protein (50 μg) was run on 10% SDS-PAGE. pEGFR, phosphorylated EGFR; pVEGFR-2; phosphorylated VEGFR-2.